Desalination and Water Treatment
www.deswater.com

doi: 10.5004/dwt.2021.27735

239 (2021) 41–53
November

Integration of Al_2O_3, CuO, and TiO_2 nanofluids for efficient solar desalination

Ibtissem Elzemzmi, Khaoula Hidouri*, Bechir Chaouachi, Hiba Akrout

Research Unit of Energy, Water, Environment and Processes, National Engineering School of Gabes, Omar Ibn El Khattab Avenue, Gabes 6029, Tunisia, emails: khaoula2013@yahoo.fr (K. Hidouri), zemzmi.ibtissem@gmail.com (I. Elzemzmi), bechir.chaouachi@enig.rnu.tn (B. Chaouachi), akrouthiba@gmail.com (H. Akrout)

Received 25 January 2021; Accepted 18 August 2021

ABSTRACT

This paper aims at the integration of Al_2O_3, CuO, and TiO_2 nanofluids for two configurations of solar desalination (SS distillation: SS with and without nanoparticle, named SSWN, SS respectively; and SS hybrid with and without nanoparticle, named SSHWN and SSH, respectively). In order to improve the productivity of a SS, a nanoparticle Al_2O_3 is integrated with different concentrations (1%, 3% and 5%). The results show very well that the addition of nanofluid regardless of the configurations of SS increases the cumulative productivity whatever the SSHWN or SSWN configuration is important compared to that of SS and SSH (SSHWN admits a P_{cu} equal to 10.8 kg/m² h and of the order of 1.6 kg/m² h for SSWN) while P_{cu} does not exceed 6.8 kg/m² h with SSH and 0.45 kg/m² h with SS configuration. We also notice that P_{cu} increases with the increase in the concentration of nanoparticles (5% the P_{cu} is 10.8 kg/m² h for SSHWN and does not exceed 6 kg/m² h SSH) the theoretical study well predicts the experimental results as regards the evolution of P_{cu}. The experimental study with different nanoparticles such as TiO_2 and CuO with a concentration of 5% shows P_{cu} (Al_2O_3) > P_{cu} (TiO_2) > P_{cu} (CuO). The thermal conductivity for hybrid solar still for different volume fractions of nanofluid has been proved. Al_2O_3 admits the highest thermal conductivity (k_{nf}/k_{bf}) the highest equal to 1.249 than that of CuO with 1.245 and finally TiO_2 1.205. A comparative study was carried out with that the correlations of Maxwell and Bruggeman gives a very good linear regression than that of our work (R^2 = 0.99).

Keywords: Solar still; Nanoparticle; Cumulated productivity; Thermal conductivity

1. Introduction

Most technological advances in solar thermal desalination focus on optimizing the following aspects: process economy, operational reliability, and process dependence on climatic conditions and elevations in the operational area. Researchers are actively exploring technological solutions such as nanoparticles, for improved conversion of solar irradiation into thermal energy to generate water vapors. An experimental study was carried out by Arani et al. [1] for tubular solar still with doping of SiO_2 nanoparticles in black paint with different concentrations ranging from 10% to 40%. They showed an increase in the heat transfer between the absorbent plate and the water. The temperature of basin and water were improved by 10.49% and 10.88%, respectively, during the use of black paint with SiO_2 nanoparticles at the concentration of 20% and they also showed that the use of the fins on the absorbent plate improved the drinking water production by 55.18% when using the nanoparticles of SiO_2 at 20% compared to that of conventional total suspended solids.

In the same context, another work was done by Panchal et al. [2] for SS with MnO_2 doping in stainless steel, with the aim of increasing efficiency. The use of this type of material for different concentrations ranges from 20% to 50%.

* Corresponding author.

This yield increases by 19.5% for the SS case with nanoparticles. The work of Essa et al. [3] was carried out for two types of SS a stepped still was taken as a reference with another modify by installing fixed suspended trays on the vertical walls of the steps to increase the surfaces. The performance of this type of still has been made for different fan speeds. For these conditions, the authors noted that the productivity increases by 4,175 against 3,800 mL/m^2/d for the reference still with an improvement of 9.8%. In addition, the use of the hanging trays and the Al_2O_3/paraffin mixture in the parallel cavity increases the productivity of the SS by approximately 40%, where the productivity was 5,740 and 4,100 mL/m^2/d for the staged stills and benchmark, respectively [4–7]. Shanmugan et al. [8] were for the goal of making SS with the coating technique using different TiO_2 and Cr_2O_3 nanoparticles. Analysis of this work was conducted by scanning electron microscopy, Fourier-transform infrared spectroscopy and X-ray diffraction. The average system output was 57.16% and 36.69% during summer and winter, respectively. The use of TiO_2 in an SS was also the objective of the work carried out by Parikh et al. [9] and this product was used as paint in the basin. The performance attains 20%–40% with black paint and with TiO_2 paint. A study on the variation of water depth was also made in this work they showed that the productivity of solar energy still increases up to a certain limit. We find that compared to the SS, 11%–18% and 20%–23% increase in productivity with a mixture of 20% and 40%. Studies were carried out for passive and hybrid SS with nanofluids (Al_2O_3–CuO) with concentrations of 0.025% for each nanoparticle. The results show a significant increase between the two stills during the months of summer and winter, that is, 5.5239 kg/m^2 h in summer and 3.1079 kg/m^2 h in winter, moreover the average exergy efficiency is increased by 22.5% in summer and 13.4% in winter thanks to the use of the nanohybrid [10].

Sharshir et al. [11] have shown a theoretical analysis of modified SS (MSS) using micro/nanoparticles to improve thermal performance. They are estimated the energy and exergy productivities for improvement to the SS. It is improved by 41.18% and 32.35% for graphite, CuO and compared with SS. The exergy efficiency of SS is 4.32% and 3.78% for graphite, CuO and CSS is 2.63%. It is valued the costs of solar still with and without micro/nanoparticles.

Zanganeh et al. [12] were developed as condensing cover of SS and were coated in condensation surface by a nano-silicon solution. It is used in nano-coating to condensate manufacturing of solar to grow significantly and verified in AFM tests of condensing cover effects dripping with 23%.

The experimental realization was carried out two configurations of SS without and with nanoparticles named SS and SSWN respectively and on the other hand a simple solar hybrid with and without nanoparticles named SSHWN and SSH respectively. This work was carried out during the month of 24–26 May 2020 at the National Engineering School of Gabès (ENIG) in the southwest of Tunisia. Following these the effect of the addition of different nanoparticles on the productivity of the two configurations was made, the effect of the variation of the concentration was followed. Thermal conductivity was measured throughout these experiments. Finally, to validate this study, we developed a MATLAB code so that we can know the validity of the different experimental results.

2. Experimental study

The SS was built in the Laboratory of Energy, Water, Environment and Processes at the National Engineering School of Gabès (ENIG). The experimental works were carried out during the month of May 2020. SS consists of a basin lined with a 0.7 mm thick galvanized iron sheet painted black to which salt water is added. The seawater is heated and evaporated by the energy of solar radiation transmitted through a glass cover 3 mm thick, then absorbed by the basin. The water vapor is then condensed at the level of the glass and the distilled water is collected. Heat loss is reduced by 2.5 cm thick glass wool insulation. The SS has side mirrors to improve productivity through the re-reflectivity of the rays on the water surface. The SS works with solar energy it is hybrid by a heat pump with a power compressor (SSH). The evaporator is in the form of a plate and is protected from solar radiation by a separation wall. Schematics and Photos of SS and SSH are shown in Figs. 1a, b and 2 (for the conventional configurations the heat pump it is closed).

Tables 1 and 2 give the various specific and operating characteristics of the SS. The distilled water produced is collected using a collecting channel at the bottom of the basin. It is important to note that the heating of the base water (seawater) is carried out both by solar radiation and by the heat pump. The dimensions of the solar still and the material properties are shown in Tables 1 and 2.

The experimental measurements of the parametric variables, water temperature, water level and relative air humidity and temperature at the basin inlet and water surface, have been recorded during the experiments. Details of all measuring equipment are tabulated in Table 1. The water temperature in the basin is measured using the thermometer-Pt100 which works in the range from −20°C to +26°C with an uncertainty of 2.6%. The relative humidity and temperature of air streams are measured using 2 thermo-hygrometers which work in the range from 0% to 100% RH and from −40°C to +12°C and its uncertainty is 1.4% (Table 3).

Nanofluids are dispersions of particles of nanometric size (whose diameter is typically less than 100 nm), called nanoparticles. Table 2 gives an idea about nanoparticles used in this work for solar distillation (Al_2O_3, CuO, and TiO_2). In the case of heat transfer fluids, one of the first parameters to take into account in order to assess the heat exchange potential is thermal conductivity. However, the most widely used fluids such as water, oil or ethylene glycol have only a low thermal conductivity compared to that of crystalline solids. The idea is then to insert nanoparticles into the base fluid in order to increase the effective thermal conductivity of the mixture. This nanofluid term was introduced by so many research works [13–15] and remains commonly used to denote this type of suspension. Fig. 3 shows the various different types of nanoparticles which are used in our works. The thermal physical properties of different nanoparticles that be used in this work are shown in Table 4.

In this approach, the nanoparticle is initially produced or purchased as a dry powder and then dispersed in the

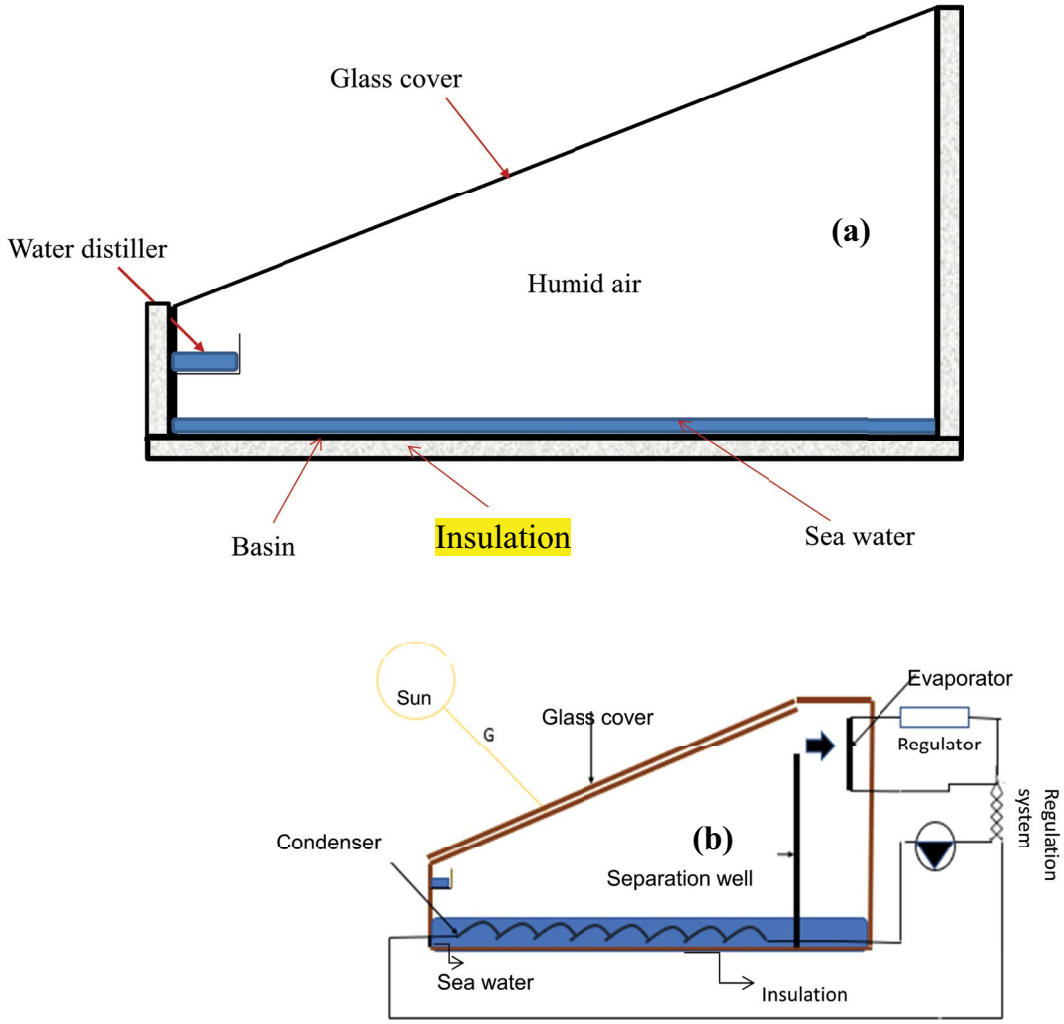

Fig. 1. Schematic diagram of (a) SS and (b) SSH.

Fig. 2. Photo of SSH.

base fluid. Nanoparticles in the base fluid are stirred using a magnetic stirrer or ultrasonic bath. In order to make the fluid and nanoparticle mixture homogeneous, Fig. 4 shows an example of the schematic procedure of the two-step approach used to synthesize nanofluid at this work. Ultrasonic agitation sonication, which is a physical method that depends on employing ultrasonic waves through the fluid, can be used to enhance the stability of the nanofluid by rupturing the nanoparticle attraction force within the sediments. Two types of ultrasonicator are used, the probe type and the bath type. Both types can be seen in our study (Fig. 5). The ultrasonic bath provides a weak sonication with approximately 20–40 W/L, while the probe-type ultrasonic can easily couple approximately 20 kW/L into the processed medium. This means that an ultrasonic probe-type exceeds an ultrasonic bath by a factor of 1,000 due to a focused and uniform ultrasonic power input [16].

3. Mathematical modeling

This part aims to develop a mathematical model describing solar distillation by means of a (SS), at first time and

hybrid (SSH) at the second time, in the presence of nanoparticle added to seawater SSWN, SSHWN. This model is used to determine the temperatures of the various components of the solar still, the hourly productivity of distilled water as well as the variation of the thermal conductivity.

3.1. Energy balance on the basin

The basin liner receives and absorbs most of the solar radiation, transfers part to the nanofluid in the form of convective heat and gives up part to the atmosphere in the form of conductive heat. The thermal balance on the basin is given in Fig. 6.

The energy stored by the basin liner can be described by this equation [17].

$$\frac{m_b C_{\mathrm{pb}}}{S_B}\frac{dT_b}{dt} = \tau_g \tau_{\mathrm{nf}} \alpha_b G - q_{c,b-\mathrm{nf}} - q_{\mathrm{loss}} \tag{1}$$

where

$$q_{c,b-\mathrm{nf}} = h_{c,b-\mathrm{nf}}\left(T_b - T_{\mathrm{nf}}\right) \tag{2}$$

The convective heat transfer coefficient between the basin and water $h_{c,b-\mathrm{nf}}$ is given by Khaoula and Mohanraj [17]:

$$h_{c,b-\mathrm{nf}} = \frac{k_{\mathrm{nf}}}{L}\mathrm{Nu} = \frac{k_{\mathrm{nf}}}{L}0.54\left(\mathrm{GrPr}\right)^{0.25} \tag{3}$$

The Grashoff (Gr) number it is given by Akrout et al. [18]:

$$\mathrm{Gr} = \frac{\beta_{\mathrm{nf}} g \rho_{\mathrm{nf}}^2 L^3 \left(T_b - T_{\mathrm{nf}}\right)}{\mu_{\mathrm{nf}}^2} \tag{4}$$

The Prandtl number is given by Dhivagar et al. [19]:

$$\mathrm{Pr} = \frac{\mu_{\mathrm{nf}} C_{\mathrm{Pnf}}}{\lambda_{\mathrm{nf}}} \tag{5}$$

Table 1
Characteristic specifications of the hybrid solar still

Specifications	Dimensions
Basin surface	0.22 m²
Glass surface	0.6 m²
Glass thickness	6 mm
Number of glass	1
Window tilt	30°

The effective thermal conductivity of a two-phase mixture consisting of continuous and discontinuous phases determined by Maxwell is found to be [20].

$$k_{\mathrm{nf}} = k_{\mathrm{bf}} \frac{\left(k_{\mathrm{np}} + 2k_{\mathrm{bf}}\right) + 2\phi\left(k_{\mathrm{np}} - k_{\mathrm{bf}}\right)}{\left(k_{\mathrm{np}} + 2k_{\mathrm{bf}}\right) - \phi\left(k_{\mathrm{np}} - k_{\mathrm{bf}}\right)} \tag{6}$$

The effective improvement in thermal conductivity was defined as the ratio of the thermal conductivity of the nanofluid to the thermal conductivity of the base fluid ($k_{\mathrm{nf}}/k_{\mathrm{bf}}$). Their models of thermal conductivity are based on the research of Maxwell [18] who developed a model to estimate and evaluate the effective thermal conductivity of a suspension containing solid particles. This model gives satisfactory results taking into account the following hypotheses [21].

- Suspensions containing particles of spherical shape,
- Relative volume concentrations,
- It does not take into account the effect of particle size or shape,
- Neglect of the effect of inter-particle interactions.

Hamilton and Crosser [22] developed the Maxwell model to take into account the effect of particle shape for liquid-solid mixtures (non-spherical particles), so they introduced a shape factor *n*, of which there they discovered that

Table 2
Operating characteristics of the hybrid solar still

Settings	Value
Glass transmissivity	0.87
Water transmissivity	0.95
Basin absorptivity	0.95
Water absorptivity	0.05
Glass absorptivity	0.04
Heat capacity of the glass	1,250 (J/kg K)
Heat capacity of water	4,090 (J/kg K)
Calorific capacity of the basin	450 (J/kg K)
Thermal conductivity of the basin	79.5 (W/m K)
Thermal conductivity of water	0.6 (W/m K)
Thermal conductivity of the insulation	0.045 (W/m K)
Glass density	1,210 (kg/m³)
Density of water	1,025 (kg/m³)
Basin density	7,874 (kg/m³)

Table 3
Range and accuracy of different measuring equipment

Instrumentation	Number	Range	Accuracy
K-Type Thermocouple	5	–200°C–1,250°C	±2°C
Digital Differential Pressure Manometer	2	(±)2 bar	±2%
Digital Thermo Hygrometer	2	0%–100% RH	±1.4% RH
Thermometer-Pt100	4	−20°C–+26°C	2.6%

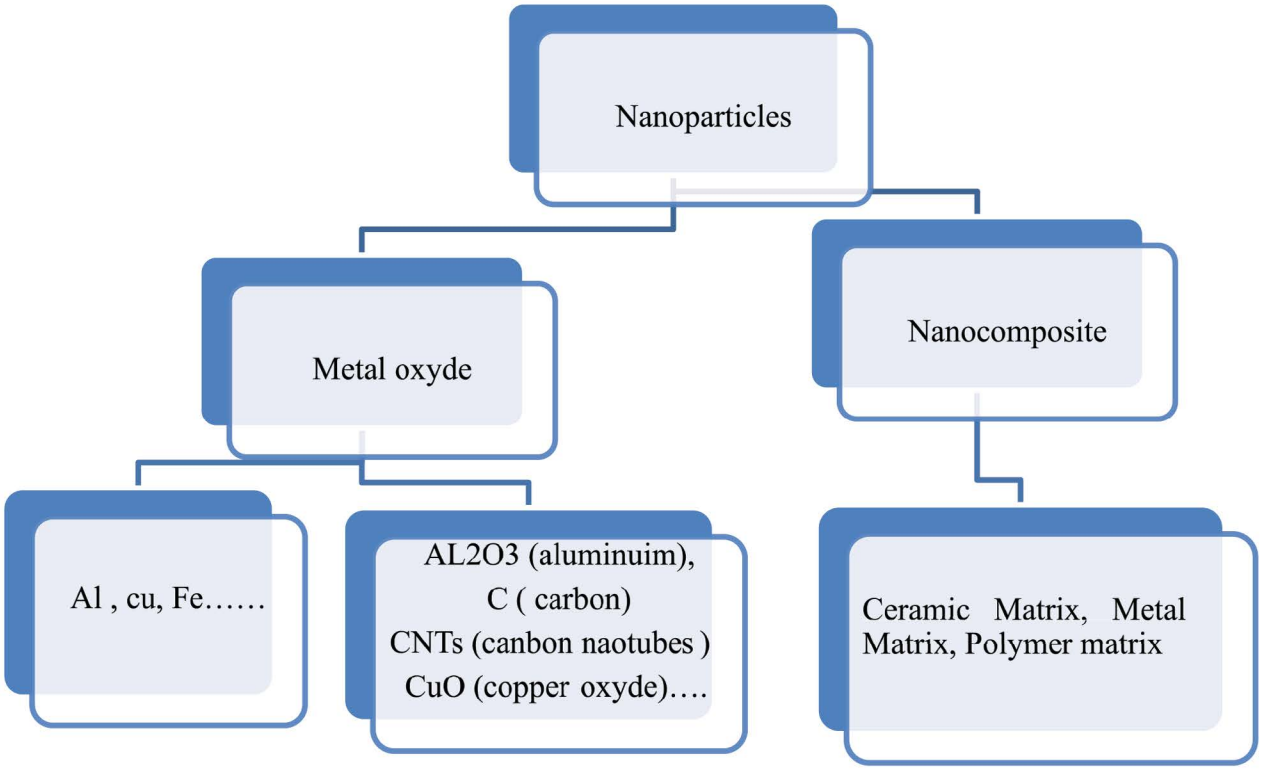

Fig. 3. Nanoparticles used in SS works [13].

Table 4
Thermophysical propriety of nanoparticles [14]

Nanoparticles	k (W/m K)	r_{np} (kg/m^3)	β_{np} (K^{-1})	Cp_{np} (J/kg K)
Al_2O_3	46	3,960	24×10^{-6}	773
TiO_2	8.4	4,230	24×10^{-6}	692
CuO	33	6,000	51×10^{-6}	551

it can be determined from experience for different types of nanoparticles.

Their study aimed to develop a model for continuous and discontinuous phases in terms of conductivity, structure and shape of nanoparticles. For the discontinuous phase diffused in the continuous phase, the Hamilton and Crosser model stated that:

$$\frac{k_{nf}}{k_{bf}} = \frac{k_{np} + (n-1)k_{bf} - (n-1)(k_{bf} - k_{np})\phi}{k_{np} + (n-1)k_{bf} + \phi(k_{bf} - k_{np})} \tag{7}$$

where n is the empirical form factor given by $n = 3/\psi$, ψ is the sphericity which is the ratio of the area of a sphere (with the same volume as the given particle) to the area of the particle, $n = 3$ for spherical particles and $n = 6$ for cylindrical particles [22].

The sphericity is 1 and 0.5 for the spherical and cylindrical shapes, respectively.

The model proposed by Zeeshan et al. [23] seems to be better approximate certain experimental results for the case of spherical nanoparticles with no limitation concerning the concentrations of the nanoparticle.

Zeeshan et al. [23] proposed this model to analyze the interactions between homogeneous spherical particles distributed in a random way.

For a binary mixture gives:

$$\frac{k_{nf}}{k_{bf}} = \frac{1}{4k_{bf}}\left[(3\phi - 1)k_s + (2 - 3\phi)k_{bf}\right] + \frac{1}{4}\sqrt{\Delta} \tag{8}$$

$$\Delta = \left[(3\phi - 1)^2\left(\frac{k_s}{k_{bf}}\right)^2 + (2 - 3\phi)^2 + 2\left(2 + 9\phi - 9\phi^2\right)\left(\frac{k_s}{k_{bf}}\right)\right] \tag{9}$$

where ϕ is the weight or concentration percentage that can be calculated with the following equation [17].

$$\phi = \frac{J_{Jnp}}{J_{np} + J_{bf}} \tag{10}$$

where J is the volume for base fluid.

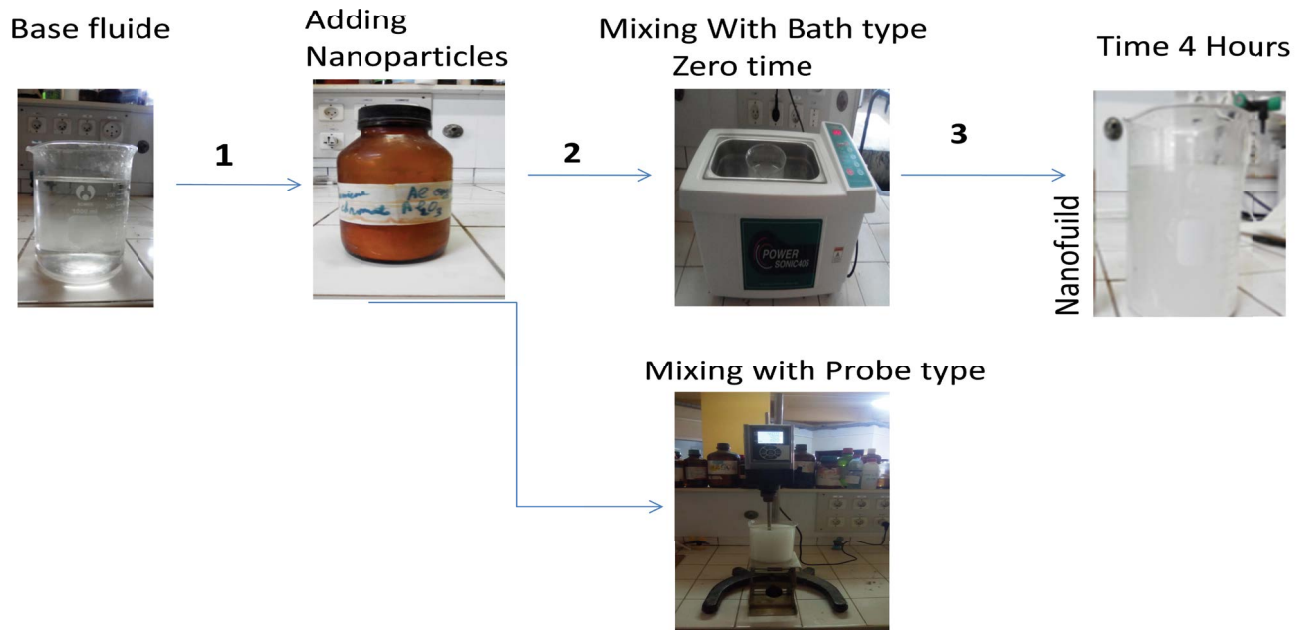

Fig. 4. Method of preparation of nanofluids.

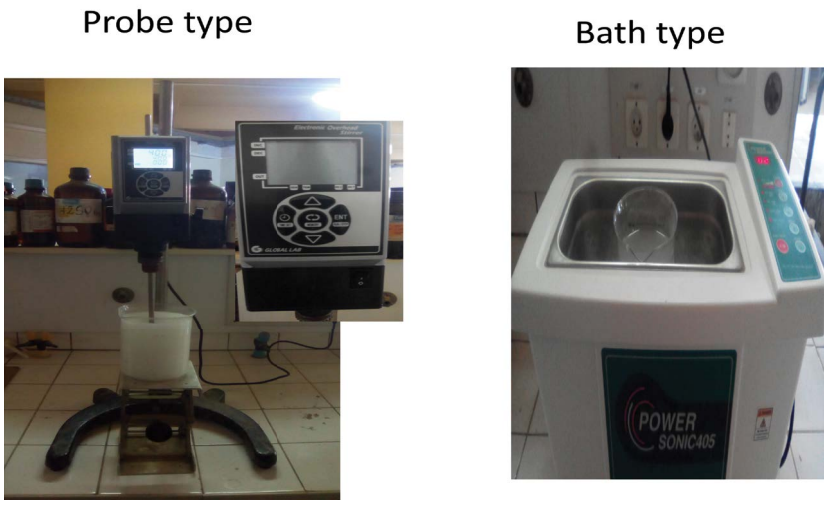

Fig. 5. Nanofluid stirring method: probe-type, ultrasonic bath ultrasound.

The effective thermal expansion of nanofluid (β_{nf}) can also be evaluated using Bruggeman [24].

$$\beta_{nf} = (1-\phi)\beta_{bf} + \phi\beta_{np} \tag{11}$$

The density of nanofluid (ρ_{nf}) is determined by Chen et al. [25].

$$\rho_{nf} = (1-\phi)\rho_{bf} + \phi\rho_{np} \tag{12}$$

The viscosity of the nanofluid (μ_{nf}) can also be determined using Eq. (14) [26].

$$\mu_{nf} = \mu_{bf}(1+2.5\phi) \quad (\text{for } \phi < 0.02\%) \tag{13}$$

The specific heat of the nanofluid (Cp_{nf}) is calculated using Eq. (15) [27].

$$Cp_{nf} = \frac{(1-\phi)Cp_{bf}\rho_{bf} + \phi Cp_{np}\rho_{np}}{\rho_{nf}} \tag{14}$$

The base fluids thermodynamics propriety it is given by Annex A.

The heat losses releases by conduction through the basin liner q_{loss} to the atmosphere are given by Eq. (16) [28].

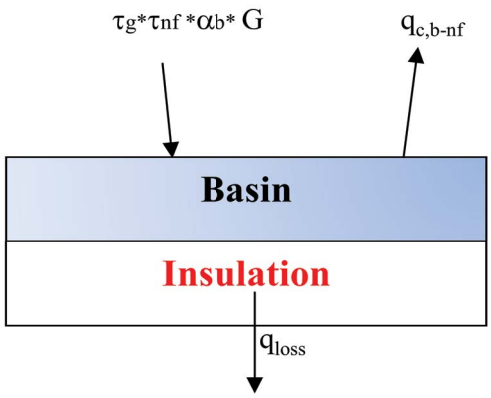

Fig. 6. Energy balance on the basin.

$$q_{\text{loss}} = \frac{K_i}{L_i}\left(T_b - T_a\right) \tag{15}$$

where K_i and L_i are respectively thermal conductivity and thickness of insulation.

3.2. Energy balance on nanofluid

The heat gained by the nanofluid it is due to the solar radiation transmitted by the glass cover, to the convective heat of the basin and the heat received from the heat pump for the hybrid model. The heat losses from the nanofluid include convective, radiative and evaporative heat to the glass cover. The thermal balance on the nanofluid is illustrated in Fig. 7.

The energy in the nanofluid it is given by Eq. (17) [29].

$$\frac{m_{\text{nf}}}{S_{\text{nf}}}\frac{C_{\text{pnf}}}{dt}\frac{dT_{\text{nf}}}{dt} = \tau_g \alpha_{\text{np}} G + q_{c,b-\text{nf}} - q_{r,\text{nf}-g} - q_{e,\text{nf}-g} - q_{c,\text{nf}-g} + q_{\text{mnf}} + q_c \tag{16}$$

The convective heat transfer rate between the nanofluid and the glass cover is given by Elsheikh et al. [30].

$$q_{c,\text{nf}-g} = h_{c,\text{nf}-g}\left(T_{\text{nf}} - T_g\right) \tag{17}$$

where $h_{c,\text{nf}-g}$ is the convective heat transfer coefficient from nanofluid to the glass cover, it can be calculated by Eq. (18) [31].

$$h_{c,\text{nf}-g} = 0.884\left[\left(T_{\text{nf}} - T_g\right) + \frac{\left(P_{\text{nf}} - P_g\right)\left(T_{\text{nf}} + 273\right)}{\left(268{,}900 - P_{\text{nf}}\right)}\right]^{1/3} \tag{18}$$

where P_{nf} and P_g are the partial pressure of the nanofluid and the cover glass, respectively, P_{nf} and P_g are given by Elsheikh et al. [30].

$$P_{\text{nf}} = \exp\left[25.317 - \left(\frac{5{,}144}{T_{\text{nf}} + 273}\right)\right] \tag{19}$$

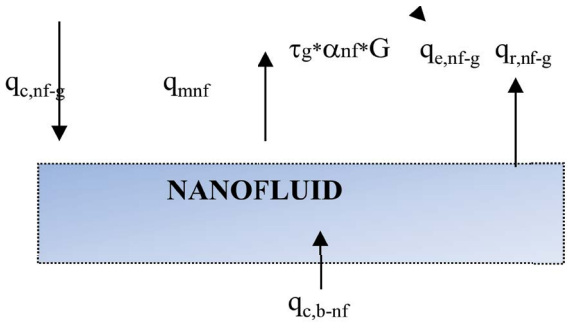

Fig. 7. Energy balance on nanofluid.

$$P_g = \exp\left[25.317 - \left(\frac{5{,}144}{T_g + 273}\right)\right] \tag{20}$$

The radiation heat transfer rate from the nanofluid to the glass cover is given by Eq. (21) [29].

$$q_{r,\text{nf}-g} = h_{r,\text{nf}-g}\left(T_{\text{nf}} - T_g\right) = \sigma\varepsilon_{\text{eff}}\left(T_{\text{nf}} + 273\right)^4 - \left(T_g + 273\right)^4 \tag{21}$$

where ε_{eff} is effective emissivity it given as Dhivagar et al. [32].

$$\varepsilon_{\text{eff}} = \left(\frac{1}{\varepsilon_{\text{nf}}} + \frac{1}{\varepsilon_g} - 1\right)^{-1} \tag{22}$$

where ε_{nf}, ε_g are emissivity of nanofluid and glass respectively.

The evaporative heat transfer rate between nanofluid and the glass cover is given by Hidouri et al. [33].

$$q_{e,\text{nf}-g} = h_{e,\text{nf}-g}\left(T_{\text{nf}} - T_g\right) = 16.273\times10^{-3} h_{c,\text{nf}-g}\left(P_{\text{nf}} - P_g\right) \tag{23}$$

The water is heated as following by q_{mnf} Sharshir et al. [34].

$$q_{\text{mnf}} = m_e\left(C_{\text{pbf}} T_{\text{bf}} - C_{\text{pa}} T_a\right) \tag{24}$$

The experimental yield is given by Eq. (25):

$$m_e = \left(\frac{h_{e,\text{nf}-g}}{h_{\text{fg}}}\right) \tag{25}$$

where h_{fg} is the heat latent, it is given as follows [35]:

$$h_{\text{fg}} = h_{r,\text{nf}-g}\left(T_{\text{nf}} - T_g\right) = 2{,}500.3 - 2.25T_{\text{nf}} - 0.02146T_{\text{nf}}^{1.5} + 3.175\times10^{-4}T_{\text{nf}}^{2.5} - 2.8610^{-5}T_{\text{nf}}^3 \tag{26}$$

3.3. Energy balance on the glass

The glass cover receiving solar radiation in the form of heat absorbs a part and allows another to pass to the basin and nanofluid assembly. The heat transfers produce by a difference of temperature, by convection, radiation and

evaporation to the glass cover. The latter, in contact with the atmosphere, will lose, by convection and radiation, heat towards the external environment. The thermal balance on the glass is illustrated in Fig. 8.

Thus, the energy stored in the glass cover is equal to the difference between the energy gained from the nanofluid and that lost in the atmosphere. It can be described mathematically using the following equation [29].

$$\frac{m_g C_{pg}}{S_g}\frac{dT_g}{dt} = \alpha_g G + q_{c,nf-g} + q_{r,nf-g} + q_{e,nf-g} - q_{r,g-a} - q_{c,g-a} \quad (27)$$

The radiative heat transfer rate between glass and sky is based on the study of Elsheikh et al. [30].

$$q_{r,g-sky} = h_{r,g-sky}\left(T_g - T_a\right) \quad (28)$$

where the coefficient of heat radiative between glass and sky is given by Eq. (29) [30].

$$h_{r,g-sky} = \varepsilon_{eff}\sigma\frac{\left(\left(T_g+273\right)^4 - \left(T_{sky}+273\right)^4\right)}{T_g - T_{sky}} \quad (29)$$

The convective heat transfer rate from glass to outside air [35].

$$q_{c,g-a} = h_{c,g-a}\left(T_g - T_a\right) \quad (30)$$

The convective heat transfer glass-ambient air coefficient [33–36].

$$h_{c,g-a} = 6.15\text{Vwin} \qquad \text{if Vwind} > \frac{5\text{m}}{\text{s}} \quad (31)$$

$$h_{c,g-a} = 2.8 + 3\text{Vwind} \quad \text{if Vwind} \le \frac{5\text{m}}{\text{s}} \quad (32)$$

Statistical analysis was used to predict the best correlation that the experimental results. For this reason, the square root of mean percent deviation (e) and coefficient of linear correlation (r) equations was used [37,38].

$$e = \sqrt{\frac{\sum_{i=1}^{n} ei^2}{N}} \quad (33)$$

$$e_i = \left(\frac{x_i - y_i}{x_i}\right)\times 100 \quad (34)$$

where x_i, y_i and N are the experimental parameters.

4. Experimental results

Fig. 9 represents the hourly variation of solar flux. The experimental result clearly shows that the solar it is maximum in the interval 11:14 TSV with a maximum is 900 W/m². The theoretical result is in good agreement with

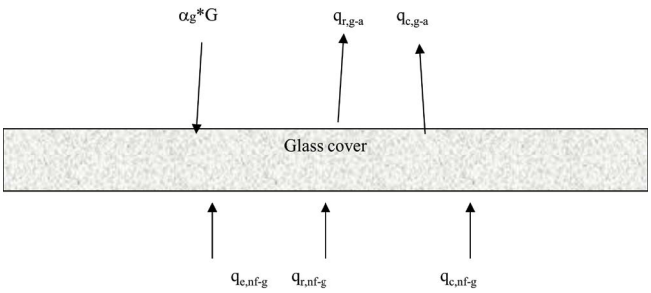

Fig. 8. Energy balance on glass.

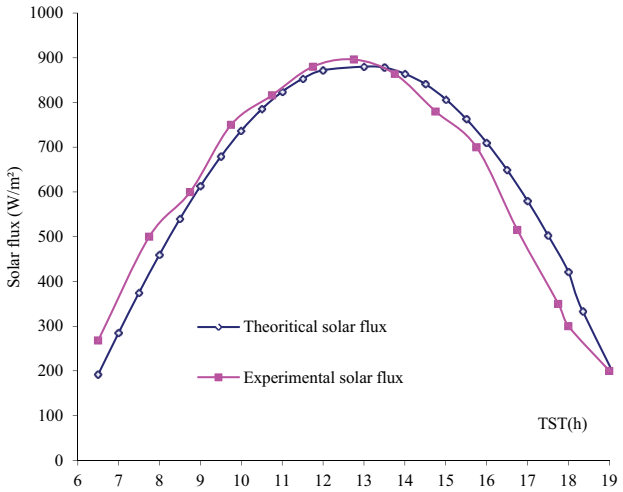

Fig. 9. Hourly variation of solar flux in 24 May 2020.

experience during the period of work. The evolution of the ambient temperature for different nanofluids is shown in Fig. 10, and we notice that the temperature is maintained almost constant throughout the day for the work.

Fig. 11 shows the cumulated productivity of SS and SSH. SSH Experimental results show clearly that the hybrid model with nanoparticles gives higher cumulative productivity (P_{cu}), that is, 5 times higher at 18 TSV compared with SS without nanoparticles (6 kg/m² h for SSH and not exceed 0.45 kg/m² h for SS).

The addition of nanoparticles is given by Fig. 12a and b for the two configurations SSWN (SS with nanoparticle) and SSHWN (SS hybrid with nanoparticle). One notices an important increase in the cumulated productivity whatever the configuration, for the case SSWN increases to reach 1.6 kg/m² h with the concentration 0.05. Regarding SSHWN, the cumulative productivity P_{cu} becomes equal to 10.83 kg/m² h for the same concentration 0.05.

The different study concentrations which are 0.01, 0.03 and 0.05 they are shown in Fig. 13a and b. Increasing the concentration results in an increase in cumulative productivity. The SSWN configuration gives 1.1 kg/m² h for a 0.01 concentration and increases to reach 1.6 kg/m² h for the 0.05 concentration. Whereas for the SSHWN configuration the cumulative productivity is equal to 8.24 kg/m² h for 0.01 concentration and exceeds 10.8 kg/m² h for a concentration of 0.05 [36–38].

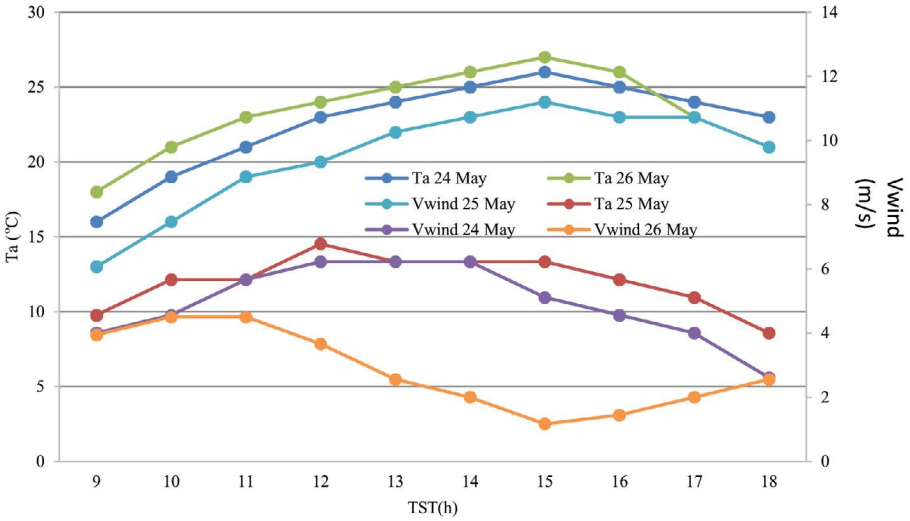

Fig. 10. Variation of ambient temperature (T_a) and wind velocity (V_{wind}).

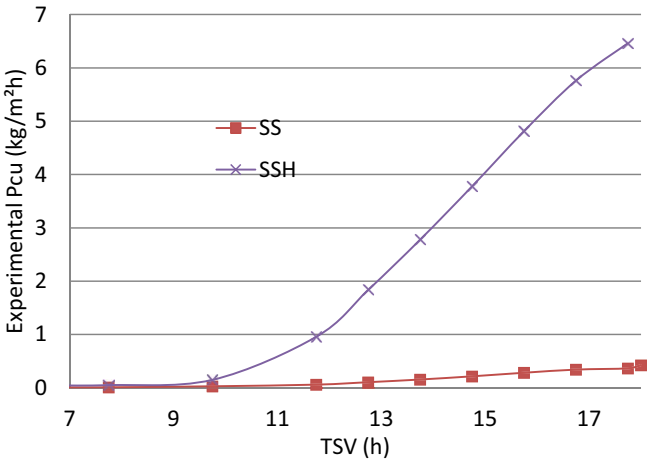

Fig. 11. Experimental cumulated productivity P_{cu} of SS and SSH configurations.

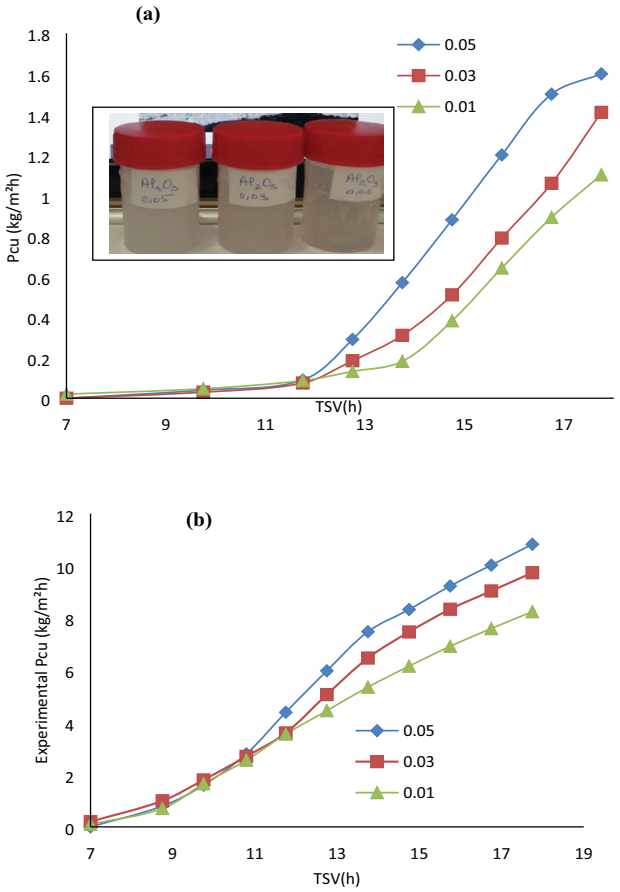

Fig. 12. (a, b) Experimental cumulated productivity for SSWN SSHWN configurations with Al_2O_3 for different concentration.

Fig. 14 gives an idea of our theoretical study which was carried out in order to know the similarity with that of the experiment. One notices a very good agreement between the experimental and theoretical results for the two configurations SSWN and SSHWN.

To find out about the influence of the nature of the nanoparticle on the productivity of SSHWN, TiO_2 and CuO nanoparticles are added with the same concentration as that of Al_2O_3 (i.e., 0.05) to make a comparison between them Fig. 13 shows that P_{cu} (Al_2O_3) > P_{cu} (TiO_2) > P_{cu} (CuO) a result which agrees very well with that of Rashidi et al. [39].

The calculations of the standard deviation agree with many research works [40–42] for the SSHWN configuration for the Al_2O_3 of an increase of 30%, around 21% for TiO_2 and in the range of 10% as regards the CuO.

At the level of Fig. 15a–c we compare the results, giving k_{nf}/k_f as a function of ϕ for the nanofluids (Al_2O_3/water, CuO/water and TiO_2/water) respectively obtained by the different models described. It emerges from this comparison that the Hamilton–Crosser model provides the highest predictions for $\psi = 0.3$.

For $\psi = 1$, we observe that the model of H-C returns to the model of Maxwell, and the values drawn from the

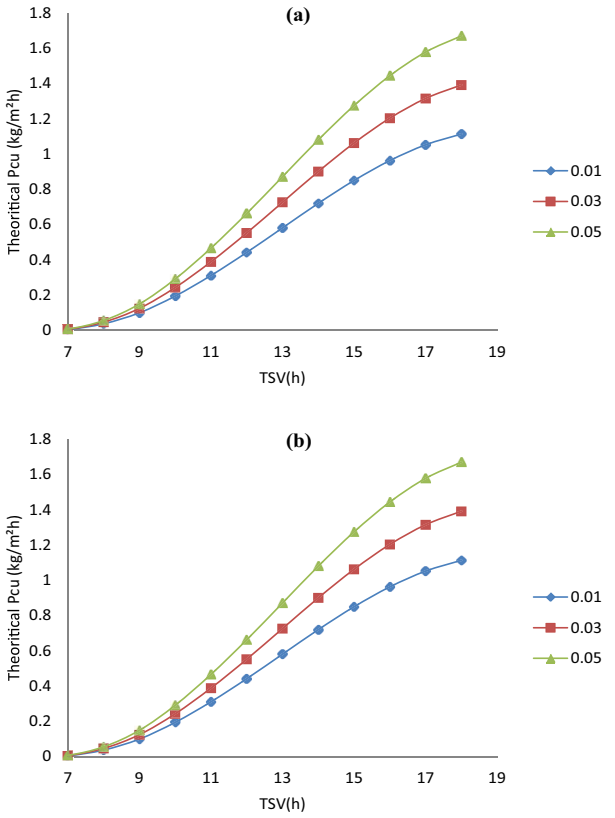

Fig. 13. (a, b) Theoretical cumulated productivity for SSWN SSHWN configurations with Al_2O_3 for different concentration.

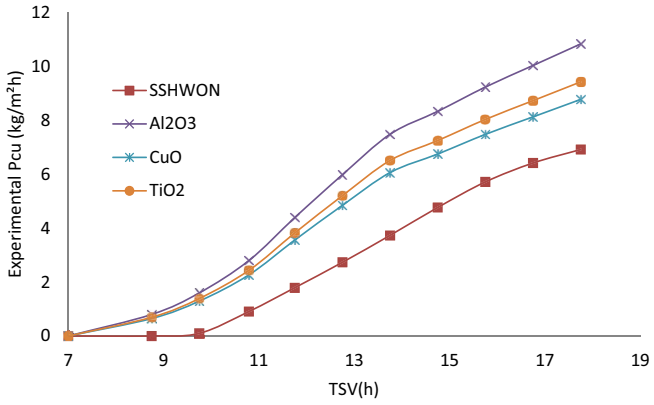

Fig. 14. Experimental variations of cumulated productivity with Al_2O_3, CuO, TiO_2 for 0.05 concentration.

model of Bruggeman are situated between those drawn from the model of H-C and that of Maxwell. The results clearly show that the thermal conductivity of metal oxide nanofluid increases linearly with the concentration of nanoparticles. These results of the current survey are validated with the previous results obtained by Singh et al. [43].

For the different fractions of nanoparticles on which we based our work and according to the model of Maxwell, we have shown that Al_2O_3 admits the highest thermal conductivity with 1.249 as the thermal conductivity ratio to that of the fluid base, then that of CuO with a 1.245 thermal

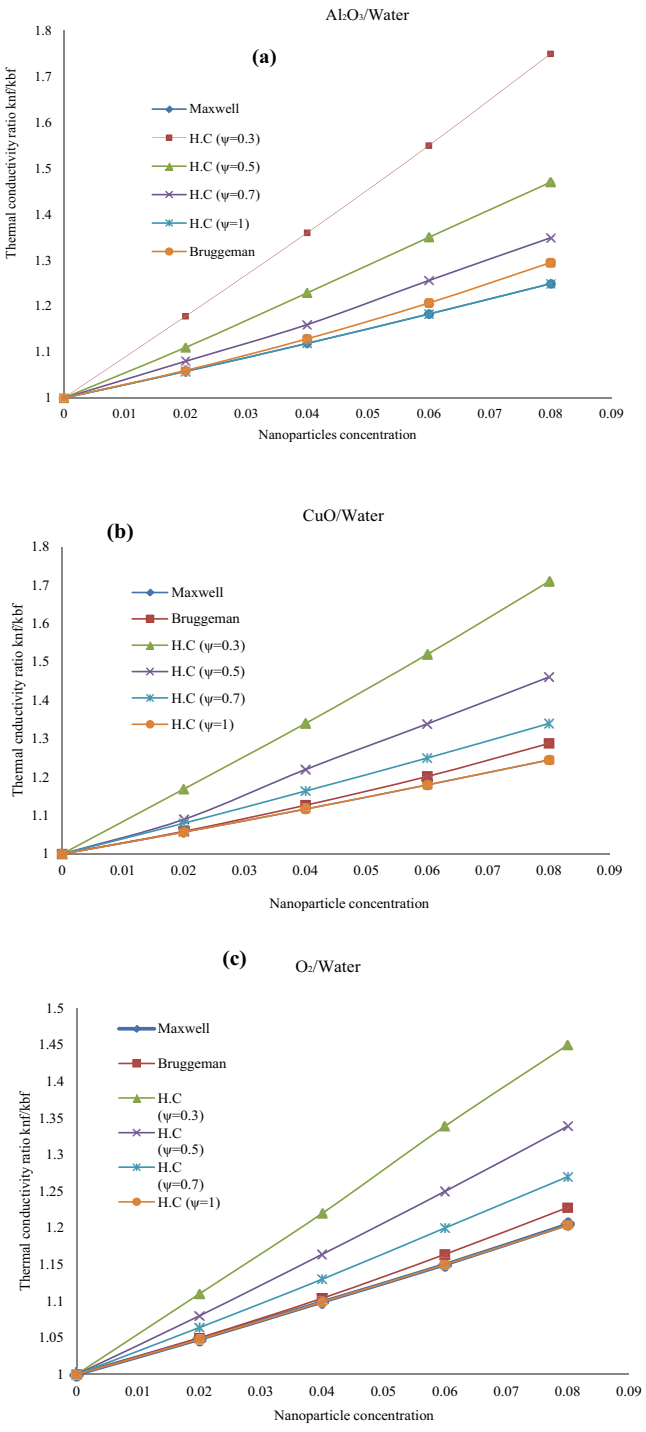

Fig. 15. (a–c) Comparison between the prediction of the H.C model with the results of the Maxwell and Bruggeman models using Al_2O_3, CuO and TiO_2.

conductivity ratio and finally that of TiO_2 with 1.205 at 0.05% as nanoparticle concentration (Fig. 16).

5. Conclusion

In order to improve the cumulated productivity (P_{cu}) for SS and SSH, the addiction of nanoparticles it

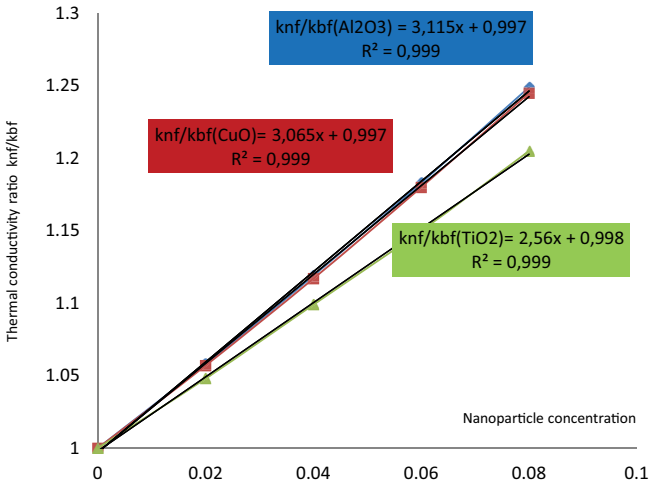

Fig. 16. Comparison between the prediction of the different nanoparticles (Al_2O_3, CuO and TiO_2) according to the Maxwell model.

be done with Al_2O_3 and with different concentrations. Experimental results show clearly that the hybrid model without nanoparticles gives higher cumulative productivity (P_{cu}) compared with SSWON (6 kg/m² h for SSH and not exceed 0.45 kg/m² h for SS). On other hand to make comparison with some other nanoparticle such us of, CuO and TiO_2 at same concentration the results have shown that the P_{cu} increase with the increase of concentration (The SSWN configuration gives 1.1 kg/m² h for a 0.01 concentration and increases to reach 1.6 kg/m² h for the 0.05 concentration. For the SSHWN configuration, the cumulative productivity is equal to 8.24 kg/m² h for 0.01 concentration and exceeds 10.8 kg/m² h for a concentration of 0.05. The addiction of nanoparticle to the base fluid has been proven to increase the thermal conductivity and improve conduction heat transfer in nanofluids compared to that in base fluid without nanoparticles (Al_2O_3 have the highest thermal conductivity with 1.249 as the thermal conductivity ratio to that of the fluid base, then that of CuO with a 1.245 thermal conductivity ratio and finally that of TiO_2 with 1.205 at 0.05% as nanoparticle concentration).

Symbols

COP	—	Coefficient of performance
Cp	—	Specific heat, J/kg K
G	—	Solar radiation, W/m²
g	—	Gravity acceleration, m/s²
h	—	Heat transfer coefficient, W/m² K
h_{fg}	—	Enthalpy of evaporation, J/kg
S	—	Area, m²
k_{nf}	—	Effective thermal conductivity (W/m K)
k_{bf}	—	Thermal conductivity of the base fluid (W/m K)
k_{np}	—	Thermal conductivity of nanoparticles (W/m K)
k	—	Thermal conductivity, W/m K
L_i	—	Thickness, m
L	—	Characteristic length, m
m	—	Mass, kg
m_e	—	Mass output, kg/m² h
P	—	Partial pressure, Pa
P_h	—	Hourly productivity
Pr	—	Prandtl number
q	—	Heat transfer rate, W/m²
Ra	—	Rayleigh number
t	—	Time, s
T	—	Temperature, °C
V_{wind}	—	Wind speed, m/s
SSHWN	—	Simple solar hybrid with nanoparticle
SSWN	—	Simple solar with nanoparticle
SS	—	Simple solar still
CSS	—	Conventional solar still
SSWON	—	Simple solar still without nanoparticle
W	—	Compressor power

Greek

α	—	Absorptivity
ε	—	Emissivity
ρ	—	Density, kg/m²
μ	—	Dynamic viscosity, N/m² s
ϕ	—	Nanoparticle concentration
ε_{eff}	—	Nanofluid-glass effective emissivity
σ	—	Stefan–Boltzmann constant, W/m² K⁴
β	—	Thermal expansion coefficient
τ	—	Transmissivity

Subscripts

a	—	Ambient
b	—	Basin
bf	—	Base fluid
c	—	Convection
e	—	Evaporative
r	—	Radiative
g	—	Glass
mnf	—	Mass of nanofluid
nf	—	Nanofluid
np	—	Nanoparticle
sky	—	Sky
i	—	Insulation
w	—	Water

References

[1] R.P. Arani, R. Sathyamurthy, A. Chamkha, A.E. Kabeel, M. Deverajan, K. Kamalakannan, M. Balasubramanian, A.M. Manokar, F. Essa, A. Saravanan, Effect of fins and silicon dioxide nanoparticle black paint on the absorber plate for augmenting yield from tubular solar still, Environ. Sci. Pollut. Res. Int., 28 (2021) 35102–35112.
[2] H. Panchal, H. Nurdiyanto, K.K. Sadasivuni, S.S. Hishan, F.A. Essa, M. Khalid, S. Dharaskar, S. Shanmugan, Experimental investigation on the yield of solar still using manganese oxide nanoparticles coated absorber, Case Stud. Therm. Eng., 25 (2021) 100905, doi: 10.1016/j.csite.2021.100905.
[3] F.A. Essa, Z.M. Omara, A.S. Abdullah, S. Shanmugan, H. Panchal, A.E. Kabeel, R. Sathyamurthy, W.H. Alawee,

A. Muthu Manokar, A.H. Elsheikh, Wall-suspended trays inside stepped distiller with Al_2O_3/paraffin wax mixture and vapor suction: experimental implementation, J. Energy Storage, 32 (2020) 102008, doi: 10.1016/j.est.2020.102008.
[4] A.E. Kabeel, R. Sathyamurthy, A. Muthu Manokar, S.W. Sharshir, F.A. Essa, A.H. Elshiekh, Experimental study on tubular solar still using graphene oxide nanoparticles in phase change material (NPCM's) for fresh water production, J. Energy Storage, 28 (2020) 101204, doi: 10.1016/j.est.2020.101204.
[5] F.A. Essa, A.S. Abdullah, Z.M. Omara, Rotating discs solar still: new mechanism of desalination, J. Cleaner Prod., 275 (2020) 123200, doi: 10.1016/j.jclepro.2020.123200.
[6] Z.M. Omara, A.E. Kabeel, A.S. Abdullah, F.A. Essa., Experimental investigation of corrugated absorber solar still with wick and reflectors, Desalination, 381 (2016) 111–116.
[7] A.S. Abdullah, F.A. Essa, Z.M. Omara, Y. Rashid, L. Hadj-Taieb, G.B. Abdelaziz, A.E. Kabeel, Rotating-drum solar still with enhanced evaporation and condensation techniques: comprehensive study, Energy Convers. Manage., 199 (2019) 112024, doi: 10.1016/j.enconman.2019.112024.
[8] S. Shanmugan, F.A. Essa, S. Gorjianc, A.E. Kabeel, R. Sathyamurthy, A. Muthu Manokar, Experimental study on single slope single basin solar still using TiO_2 nano layer for natural clean water invention, J. Energy Storage, 30 (2020) 101522, doi: 10.1016/j.est.2020.101522.
[9] R. Parikh, U. Patdiwala, S. Parikh, H. Panchal, K. K. Sadasivuni, Performance enhancement using TiO_2 nanoparticles in solar still at variable water depth, Int. J. Ambient Energy, (2021), doi: 10.1080/01430750.2021.1873853.
[10] E.F. El-Gazar, W.K. Zahra, H. Hassan, S.I. Rabia, Fractional modeling for enhancing the thermal performance of conventional solar still using hybrid nanofluid: energy and exergy analysis, Desalination, (2021), doi: 10.1016/j.desal.2020.114847.
[11] S.W. Sharshir, P. Guilong, A.H. Elsheikh, E.M.A. Edreis, A.M. Eltawil, T. Abdelhamid, E.A. Kabeel, J. Zang, N. Yang, Energy and exergy analysis of solar stills with micro/nanoparticles: a comparative study, Energy Convers. Manage., 177 (2018) 363–375.
[12] P. Zanganeh, A.S. Goharrizi, S. Ayatollahi, M. Feilizadeh, Productivity enhancement of solar stills by nano-coating of condensing surface, Desalination, 454 (2019) 1–9.
[13] L. Qiu, N. Zhu, Y. Feng, E.E. Michaelides, G. Żyła, D.W. Jing, X.X. Zhang, P.M. Norris, C.N. Markides, O. Mahian, A review of recent advances in thermophysical properties at the nanoscale: from solid state to colloids, Phys. Rep., 843 (2020) 1–81.
[14] J. Nadal-Bach, J. Carles Bruno, J. Farnós, M. Rovira, Solar stills and evaporators for the treatment of agro-industrial liquid wastes: a review, Renewable Sustainable Energy Rev., 142 (2021) 110825, doi: 10.1016/j.rser.2021.110825.
[15] A. Rajendra Prasad, R. Sathyamurthy, M. Sudhakar, B. Madhu, D. Mageshbabu, A. Muthu Manokar, A.J. Chamkha, Effect of design parameters on fresh water produced from triangular basin and conventional basin solar still, Int. J. Photoenergy, 2021 (2021) 6619138, doi: 10.1155/2021/6619138.
[16] M.F. Zawrah, R.M. Khattab, L.G. Girgis, H. El Daidamony, R.E. Abdel Aziz, Stability and electrical conductivity of water-base Al_2O_3 nanofluids for different applications, HBRC J., 12 (2016) 227–234.
[17] H. Khaoula, M. Mohanraj, Thermodynamic analysis of a heat pump assisted active solar still, Desal. Water Treat., 154 (2019) 101–110.
[18] H. Akrout, K. Hidouri, A. Benhmidene, B. Chaouachi, Energetic, exergetic and entropic study in a simple and hybrid solar distiller, Int. J. Ambient Energy, (2020) 1745274, doi: 10.1080/01430750.2020.1745274.
[19] R. Dhivagar, M. Mohanraj, K. Hidouri, Y. Belyayev, Energy, exergy, economic and enviro-economic (4E) analysis of gravel coarse aggregate sensible heat storage-assisted single-slope solar still, J. Therm. Anal. Calorim., 145 (2020) 1–22, doi: 10.1007/s10973-020-09766.
[20] J.C. Maxwell, A Treatise on Electricity and Magnetism, 3rd ed., Vol. 1., Dover Publications, Inc., Mineola (NY), 1954.
[21] B. Madhu, E. Balasubramanian, P.K. Nagarajana, R. Sathyamurthy, A.E. Kabeel, T. Arunkumar, D. Mageshbabu, Improving the yield of fresh water from conventional and stepped solar still with different nanofluids, Desal. Water Treat., 100 (2017) 243–249.
[22] R.L. Hamilton, O.K. Crosser, Thermal conductivity of heterogeneous two-component systems, Ind. Eng. Chem. Fundam., 1 (1962) 187–191.
[23] A. Zeeshan, R. Ellahi, F. Mabood, F. Hussain, Numerical study on bi-phase coupled stress fluid in the presence of Hafnium and metallic nanoparticles over an inclined plane, Int. J. Numer. Methods Heat Fluid Flow, 29 (2019) 2854–2869.
[24] D.A.G. Bruggeman, Berechnung verschiedener physikalischer Konstanten von heterogenen Substanzen. I. Dielektrizitätskonstanten und Leitfähigkeiten der Mischkörper aus isotropen Substanzen, Ann. Phys. (Leipzig), 416 (1935) 636–664.
[25] W. Chen, C. Zou, X. Li, H. Liang, Application of recoverable carbon nanotube nanofluids in solar desalination system: an experimental investigation, Desalination, 451 (2019) 92–101.
[26] E. Abu-Nada, Z. Masoud, H.F. Oztop, A. Campo, Effect of nanofluid variable properties on natural convection in enclosures, Int. J. Therm. Sci., 49 (2010) 479–491.
[27] R.S. Kumar, T. Sharma, Stability and rheological properties of nanofluids stabilized by SiO_2 nanoparticles and SiO_2-TiO_2 nanocomposites for oilfield applications., Colloids Surf., A, 539 (2018) 171–183.
[28] A. Einstein, Investigations on the Theory of The Brownian Movement, Dover, New York, 1956.
[29] G. Peng, H. Ding, S.W. Sharshir, X. Li, H. Liu, D. Ma, L. Wu, J. Zang, H. Liu, W. Yu, H. Xie, N. Yang, Low-cost high-efficiency solar steam generator by combining thin film evaporation and heat localization: Both experimental and theoretical study, Appl. Therm. Eng., 143 (2018) 1079–1084.
[30] A.H. Elsheikh, S.W. Sharshir, M.K. Ahmed Ali, J. Shaibo, E.M.A. Edreis, T. Abdelhamid, C. Du, Z. Haiou, Thin film technology for solar steam generation: a new dawn, Sol. Energy, 177 (2019) 561–575.
[31] K. Hidouri, D.R. Mishra, A. Benhmidene, B.Chouachi, Experimental and theoretical evaluation of a hybrid solar still integrated with an air compressor using ANN, Desal. Water Treat., 88 (2017) 52–59.
[32] R. Dhivagar, M. Mohanraj, K. Hidouri, M. Midhun, CFD modeling of a gravel coarse aggregate sensible heat storage assisted single slope solar still, Desal. Water Treat., 210 (2021) 54–69.
[33] K. Hidouri, R. Ben Slama, S. Gabsi, Hybrid solar still by heat pump compression, Desalination, 250 (2010) 444–449.
[34] S.W. Sharshir, M.O.A. El-Samadony, G. Peng, N. Yang, F.A. Essa, M.H. Hamed, A.E. Kabeel, Performance enhancement of wick solar still using rejected water from humidification-dehumidification unit and film cooling, Appl. Therm. Eng., 108 (2016) 1268–1278.
[35] H. Khaoula, B.H. Ali, C. Bechir, R. Sathyamurthy, Comparative study for evaluation of mass flow rate for simple solar still and active with heat pump, J. Water Environ. Nanotechnol., 2 (2017) 157–165.
[36] A.H. Elsheikh, S.W. Sharshir, M.E. Mostafa, F.A. Essa, M.K. Ahmed Ali, Applications of nanofluids in solar energy: a review of recent advances, Renewable Sustainable Energy Rev., 82 (2018) 3483–3502.
[37] K. Hidouri, S. Gabsi, Correlation for Lewis number for evaluation of mass flow rate for simple/hybrid solar still, Desal. Water Treat., 57 (2015) 1–8.
[38] K. Hidouri, D.R. Mishra, Experimental evaluation of influence of air injection rate on a novel single slope solar still integrated with an air compressor, Global J. Res. Eng.: A Mech. Mech. Eng., 17 (2017).
[39] S. Rashidi, M. Bovand, N. Rahbar, J.A. Esfahani, Steps optimization and productivity enhancement in a nanofluid cascade solar still, Renewable Energy, 118 (2018) 536–545.
[40] A. Iqbal, M.S. Mohamed, E.T. Sayed, K. Elsaid, M.A. Abdelkareem, H. Alawadhi, A.G. Olabi, Evaluation of the nanofluid-assisted

desalination through solar stills in the last decade, J. Environ. Manage., 277 (2021) 111415, doi: 10.1016/j.jenvman.2020.111415.
[41] S.W. Sharshir, M.R. Elkadeem, A. Meng, Performance enhancement of pyramid solar distiller using nanofluid integrated with v-corrugated absorber and wick: an experimental study. Appl. Therm. Eng., 168 (2020) 114848, doi: 10.1016/j.applthermaleng.2019.114848.
[42] A.K.R. Singh, H.K. Singh, Performance evaluation of solar still with and without nanofluid, Int. J. Sci. Eng. Technol., 3 (2015) 1093–1101.
[43] A.K. Singh, D.B. Singh, V.K. Dwivedi, G.N. Tiwari, A. Gupta, Water purification using solar still with/without nano-fluid: a review, Mater. Today:. Proc., 21 (2020) 1700–1706.
[44] S. Rashidi, S. Akar, M. Bovand, R. Ellahi, Volume of fluid model to simulate the nanofluid flow and entropy generation in a single slope solar still, Renewable Energy, 115 (2018) 400–410.